

## Numerical Study on the Effects of Wire bonding Looping formation on Light-emitting Diode Encapsulation Process

Ahmad Amin Azmi Jaludin<sup>1</sup>, Mohd Syakirin Rusdi<sup>2</sup>, Mohd Sharizal Abdul Aziz<sup>2</sup> and Mohammad Hafifi Hafiz Ishak<sup>1\*</sup>

<sup>1</sup>*School of Aerospace Engineering, Universiti Sains Malaysia, Engineering Campus, 14300 Nibong Tebal, Seberang Perai Selatan, Penang, Malaysia*

<sup>2</sup>*School of Mechanical Engineering, Universiti Sains Malaysia, Engineering Campus, 14300 Nibong Tebal, Seberang Perai Selatan, Penang, Malaysia*

### ABSTRACT

This study focused on evaluating the effects of different wire-bonding looping formations on key mechanical properties during the encapsulation process of light-emitting diodes (LEDs). The specific properties investigated included total maximum deformation, maximum equivalent elastic strain, and maximum von Mises stress, which are critical to ensuring LEDs' structural integrity and performance under encapsulation. The encapsulation process was simulated using advanced computational methods, including Volume of Fluid (VOF), Fluid-Structure Interaction (FSI), and system coupling techniques within the ANSYS software environment. The simulations were designed to mimic the behavior of epoxy molding compound (EMC) as it interacts with various wire configurations over time, providing insights into the dynamic responses of the LED structures. These simulation results were rigorously validated against experimental data to ensure accuracy and reliability. Among the wire configurations tested, the Type 2 wire demonstrated high compatibility with the EMC, exhibiting the highest maximum strain and stress values. Conversely, the square-loop (type 3) configuration emerged as the most optimal, offering the lowest levels of total deformation, strain, and stress, thereby indicating superior overall performance. The comparative analysis ranked the wire configurations in the following order of performance with the EMC: Type 2, type 1, and type 3. These findings provide valuable insights for optimizing wire configurations in LED encapsulation processes, potentially leading to improved durability and reliability of LED devices.

### ARTICLE INFO

#### Article history:

Received: 22 August 2024

Accepted: 16 January 2025

Published: 26 March 2025

DOI: <https://doi.org/10.47836/pjst.33.3.08>

#### E-mail addresses:

[aminazmi.jaludin@student.usm.my](mailto:aminazmi.jaludin@student.usm.my) (Ahmad Amin Azmi Jaludin)

[syakirin@usm.my](mailto:syakirin@usm.my) (Mohd Syakirin Rusdi)

[msharizal@usm.my](mailto:msharizal@usm.my) (Mohd Sharizal Abdul Aziz)

[mhaffihafiz@usm.my](mailto:mhaffihafiz@usm.my) (Mohammad Hafifi Hafiz Ishak)

\*Corresponding author

**Keywords:** Encapsulation process, fluid-structure interaction, LED, wire configuration

## INTRODUCTION

LEDs are solid-state lighting (SSL) that transform power into light. LEDs are monochromatic due to the semiconductor's energy bandgap. There are various LED light varieties on the market. Common LED light types are hole-type, SMD-type, bi-color, RGB-type, and HP-LED. LEDs can replace incandescent and halogen bulbs due to their energy efficiency, low cost, extended lifespan, environmental friendliness, and portability (Hamidnia et al., 2018). LED chip packaging protects the connected wire and chip from flaws through LED encapsulation. Encapsulation and lens formation affect LED chip light extraction (Roslan et al., 2020). Silicone and epoxy resins are the principal LED encapsulating mediums. Epoxy resins are popular due to their inexpensive cost, adhesive strength, and dielectric constant. Silicone resins have outstanding thermal and optical properties, a long lifespan, and a wide working temperature range (Alim et al., 2021). The encapsulant fills the LED package cavity and encloses the bonding wires because materials have various CTEs and thermos-mechanical stress affecting LED failure (Packwood et al., 2018). Wire bonding provides communication and power between chips and substrates in LED packages. Semiconductor packaging uses gold wire bonding to connect the substrate and chip. Gold wire offers consistent chemical characteristics, good weldability, and high ductility (Tian et al., 2019). Bonding wires during LED operation help dissipate heat. Wire-bonding technologies have a limited material selection and risk bond surface defects and wear (Alim et al., 2021). LEDs use semiconductors to convert electrical energy into visible, Ultraviolet, or Infrared light (Koutchma, 2019). The region where active electrons and holes are injected is referred to as the p-n junction (Alim et al., 2020; Ünal et al., 2022).

The active layer of an LED chip captures all the electron-hole pairs and turns the output energy into optical power in the ideal circumstance. Nevertheless, some electrical energy is transformed into heat energy in the actual condition. The electrons and holes enter the active zone and combine radiatively or non-radiatively when an LED turns on. The goal of employing LED is to produce photons by radiative recombination. Meanwhile, non-radiative recombination generates heat at the active layer, and Joule heating at the interconnects and diode's series electrical resistance (Hamidnia et al., 2018). The creation of the new LED that combined the three fundamental colors to generate white light and other color temperatures made LED technology suitable for indoor illumination (Montoya et al., 2017). For LED equipment exceeding 10W, Chip-on-Board (COB) packaging is the method of choice. This technology attaches LED chips to their substrates, boosting LED performance over single-chip packaging. LED packaging is easier to make, cheaper, and smaller than normal packaging. Different levels of electrical packaging exist. The semiconductor is level zero, and its connections and encapsulation are level one. Second-level packaging connects the microelectronic package to the printed circuit board (PCB). Both single-chip and multi-chip packaging are available for two-dimensional microelectronic devices.

Encapsulated single-chip packages are lead frame and substrate. Lead-frame packages are surface-mounted or through-hole mounted to the PCB. Through-hole technology in the 1960s required package leads to be inserted into plated circuit board through-holes. Place the leads and wave solder the electrical connection. Pin-grid array (PGA), dual in-line package (DIP) and Single in-line package (SIP) are the most popular through-hole packages. Surface-mounted packages include Small-outline package (SOP), Plastic-leaded chip carrier (PLCC), Quad-flat-pack (QFP), and Ball-grid array (BGA). These packages for discrete implantation on printed wiring boards have components on both sides of the circuit board. Ball grip package (BGA), chip scale package (CSP), chip-on-board (COB), and flip chip (FC) are substrate single-chip packaged (Arriola et al., 2023).

Electronic devices commonly use T-pack LED chips, the original LED chip. However, they are weak and emit a limited amount of light. Most UV LEDs are SMD, which are attached to a printed circuit board and contain one or more chips in ceramic packaging. Chip-on-board (COB) LEDs with appropriate equipment are installed onto the circuit board (Koutchma, 2019). Despite its enormous heat dissipation area, the widely used SMD LED light has poor optical efficiency. Many COB (Chip on board) LED lamps have improved optical efficiency, but thermal issues remain, especially in applications over 100W (Moon et al., 2017). Encapsulating the LED prevented deterioration because biological molecules are susceptible to environmental factors. Various thicknesses of  $Al_2O_3$  films were produced using atomic layer deposition at 85°C to attain optimal development (Mahmood et al., 2022). Continuous oxygen and moisture exposure degrades LEDs quickly. The main causes of OLED degradation are interface delamination, organic material crystallization, electrode oxidation, and layer physical and chemical changes. The hygrothermal aging test was performed in a humidity chamber at 85°C and 85% RH using commercially encapsulated LEDs. At high temperatures, trapped moisture became a gas, and the gas expansion pressure weakened the cathode-polymer layer adhesion, causing bubble defects on the cathode's surface. Defects destroyed the aluminum film and caused the device to fail (Azrain et al., 2019).

EMC flow behavior in molds affected electronic package operation and reliability, making it important to examine. Transfer molding speed injection and stacking affected EMC flow and void formation during encapsulation. A multi-flip chip package molded underfill (MUF) was numerically investigated using ANSYS Fluent's Castro Macosko model. Shear rate and velocity profiles in the free passage and flip chip region are negatively linked to EMC viscosity (Azmi et al., 2018). Epoxy resin's bonding strength and material properties can vary with temperature. When the temperature rises, the epoxy resin of elastic modulus falls. The viscosity of epoxy and dispensed volume both had an impact on the quality of the LED package. The adhesive viscosity can be accurately estimated using the viscosity model, and the appropriate jetting temperature can be determined (Shan

& Chen, 2018). Package warpage was the main issue in packaging innovation. Surface mount technology (SMT) issues include mounting errors during chip attachment and poor solder connections between the package and PCB. The thermal properties of the epoxy molding compound (EMC), including its coefficient of thermal expansion (CTE) curing, shrinkage (CS), and viscoelastic behavior, influence the warpage. EMC viscoelasticity was measured using a three-point bending stress relaxation test. Dielectric and Fibre Bragg grating (FBG) sensors assessed EMC internal strain and recovery. EMC aluminum bi-layer strip warpage was determined via FEM simulation, which resulting EMC cure shrinkage, which is important in forecasting semiconductor warpage (Baek et al., 2022). Additionally, the encapsulant reduced the LED's brightness and color emission efficiency. Excess epoxy pressured gold wire bonding and affected the PCB-gold wire interface. Insufficient epoxy caused poor LED light output.

This research investigates how gold wire configurations influence fluid behavior and mechanical properties during LED encapsulation. Advanced simulation techniques such as Volume of Fluid (VOF) and Fluid-Structure Interaction (FSI) are employed, and the results are validated through comparison with experimental data. By exploring the effects of wire configurations, this work advances LED technology and offers valuable insights for innovative design and manufacturing approaches that enhance the durability, efficiency, and performance of LED products across various applications.

## METHODOLOGY

### Physical Model and Computational Domain

The geometry model of the LED package, featuring three different wire bonding looping formations: Type 1, Type 2 and Type 3, was created using SolidWorks and then imported into ANSYS. These wire configurations were selected due to their widespread use in the industry, each providing distinct mechanical and thermal performance characteristics. The needle tip's inner diameter is 1 mm, while the domain has a height of 4 mm and a diameter of 3 mm. The gold wire used has a diameter of 0.03 mm. The syringe and domain are considered fluid bodies, whereas the gold wires and substrates are treated as solid bodies. Figure 1 illustrates the geometry model of the Type 1 wire configuration. An isometric and front view of all three wire configurations connecting the LED chip to the substrate is depicted in Figure 2. System Coupling was employed to simulate and analyze the interaction between the epoxy material and the wires. This setup allows Fluent to address fluid dynamics while Static Structural handles wire deflection and stress analysis. During the simulation, data from the Fluent and Static Structural simulations are transferred to System Coupling, with force data moving from Fluent to Static Structural and displacement data sent from Static Structural to Fluent.

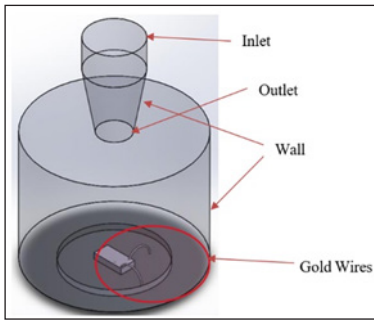


Figure 1. LED Encapsulation process geometry model

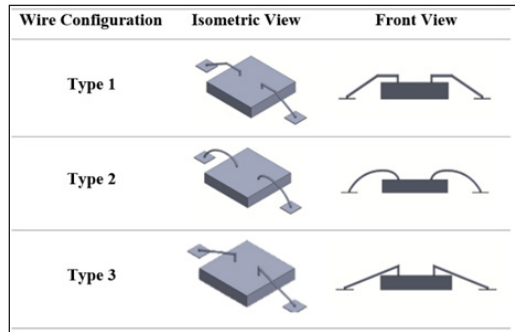


Figure 2. Isometric view and Front view of the three different types of wire configuration

The fluid domain meshes in Figure 3(a) are polyhedral and 0.10mm in size. The fluid domain has 126511 elements and 151428 nodes. Figure 3(b) shows poly-hexacore solid body meshes with 0.01mm element size. The solid body has 3366 components and 16356 nodes. In the simulation, the Volume of Fluid (VOF) is used to measure the interface between two fluids with different properties, such as air and water (Garoosi & Mahdi, 2022). The interface is where one fluid’s volume fraction goes from zero to one and the other from one to zero.

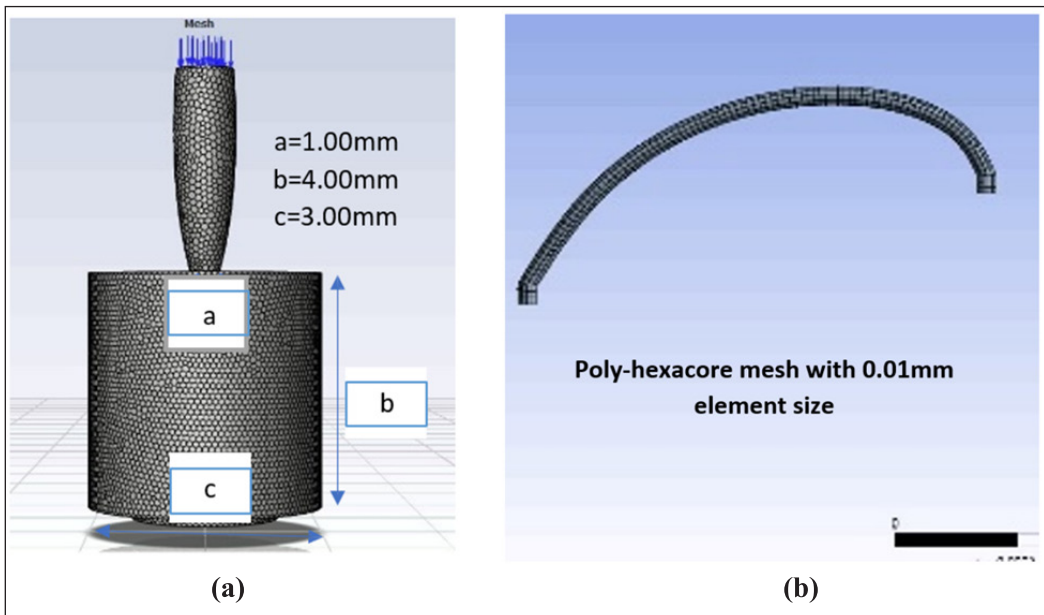


Figure 3. Mesh generation (a) fluid domain, (b) solid domain

The Laminar model was used as the viscous model. A user-defined function (UDF) was employed in the simulation to mimic the encapsulant injection motion flow process where the motion is initially important but later becomes stationary. After the setup, the data generated from the Fluent and Static Structural simulations is transferred to the System Coupling. In the system coupling, the force data is transferred from Fluent to Static Structure, while the displacement data is transferred from Static Structural to Fluent. The real-time analysis of FSI simulation is shown in Figure 4.

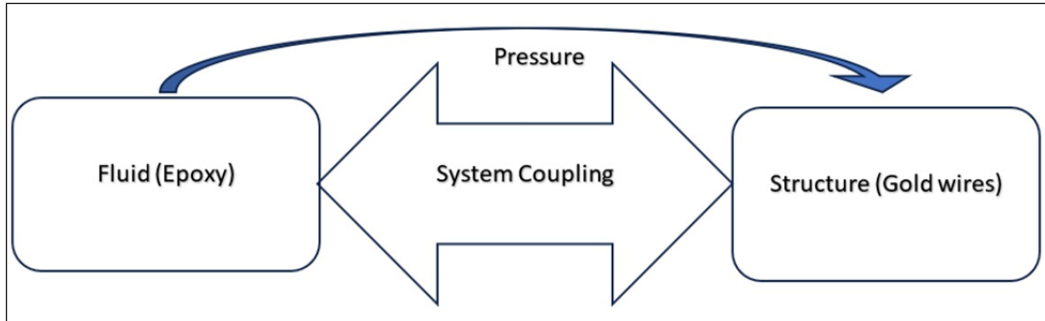


Figure 4. Concept of fluid-structure interaction analysis between epoxy and gold wires

The output analysis from the static structural simulation includes maximum total deformation, equivalent elastic strain and von Mises stress. The maximum total deformation, defined as the largest overall displacement experienced at any point within the structure, was analyzed to assess the structural response under load. The equivalent elastic strain is a scalar quantity derived from the strain tensor, representing the intensity of elastic deformation in a material. It provides a simplified measure to compare different strain states on a unified scale, helping identify areas of significant elastic deformation. Von Mises stress is a widely used criterion to determine whether a material will yield or fail under complex loading conditions. It provides a scalar value that combines the effects of different stress components acting in three dimensions, which offers a single measure to evaluate the material response.

### Material Properties and Boundary Conditions

In the simulation setup, boundary conditions and material properties for the gold wire were obtained from previous studies (Roslan et al., 2020) and the ANSYS database, as presented in Tables 1 and 2. Figure 5 displays the boundary conditions for the fluid domain and the fixed boundary for the solid model. The top surface of the needle is defined as the inlet, with the needle body and domain acting as walls. The fixed boundary is located at the wire's end in the structural analysis. The simulation uses an inlet velocity of 2 m/s and an

injection time of 3 seconds. The epoxy molding compound in the analysis has a viscosity of 0.448 kg/ms, a constant density of 1800 kg/m<sup>3</sup>, and a surface tension of 0.005 N/m.

Table 1

*Material Properties of gold wire*

Gold Wire	Unit	Properties
Density	kg/m <sup>3</sup>	193300
Young's Modulus	Pa	7.85 x 10 <sup>10</sup>
Tensile Yield Strength	Pa	1.84 x 10 <sup>8</sup>
Tensile Ultimate Strength	Pa	1.99 x 10 <sup>8</sup>
Poisson's Ratio	-	0.42
Diameter	mm	0.03

Table 2

*Boundary condition for the simulation*

Boundary Condition	Unit	Detail
Needle Diameter, a	mm	1.00
Distance of Needle to Base, b	mm	3.00
Base Diameter, c	mm	3.00
Inlet Speed	m/s	2.00
Injection time	s	0.3

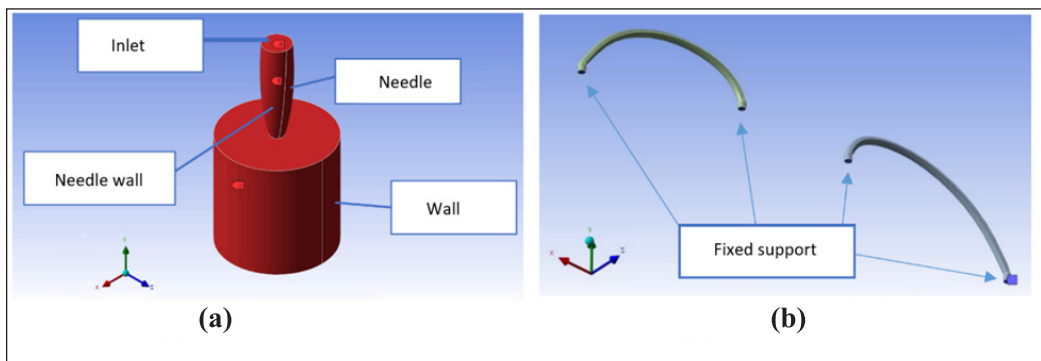


Figure 5. Boundary conditions of (a) fluid domain and (b) solid model

### Grid-independent Test

The grid-independent test ran the same simulation with multiple grid sizes or mesh refinement levels to determine the minimum mesh refinement required for an accurate solution in the simulation (Lee et al., 2020). The model used is Type 2 with 0.03mm gold wire. Five levels of refinements, which are Mesh-1 (0.10 mm), Mesh-2 (0.15 mm), Mesh-3 (0.20 mm), Mesh-4 (0.25 mm), and Mesh-5 (0.30 mm), have been analyzed to determine the optimal mesh element size for the simulation study. Figure 6 illustrates the grid-independent test for different mesh element sizes against the Von Mises Stress using the Type 2 configuration with 0.03mm gold wire. In this study, Mesh-2 with an element size of 0.15 mm was chosen for all simulations as it showed optimal results in terms of result and computing time.

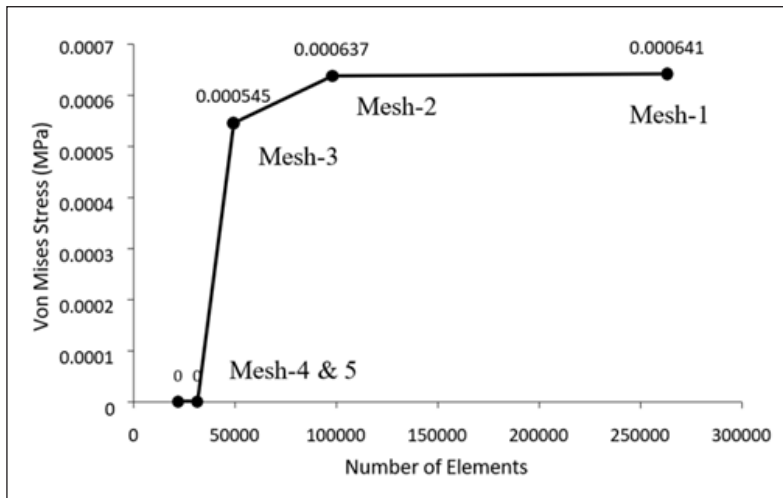


Figure 6. Grid independent test (Von Mises stress curve for different mesh counts)

### Experiment Setup

The encapsulation process plays a crucial role in protecting the LED components from environmental factors and ensuring optimal performance. Simulation techniques have been widely used to model the LED encapsulation process; however, experimental validation is essential to verify the accuracy of simulation results. In this study, an experiment is conducted to validate the LED encapsulation process using digital image analysis. The experimental setup included a micrometer, syringe, light source, laboratory stand, microscope, and monitor, all configured to achieve standardized results with minimal error, as illustrated in Figure 7. The distance between the needle tip and the substrate was controlled using a knob. The encapsulant used in the tests consists of two parts. Part A contains epoxy ( $C_{21}H_{25}ClO_5$ ), while part B serves as the hardener (Alcyclic anhydrides). Part-A and Part-B are mixed in equal volume percentages before being used as an encapsulant.

Three methods were employed to determine the average drop volume. First, twenty drops were collected in a pre-tared beaker, and the average droplet volume was calculated. Microscopic images were taken, and the droplet volume was manually calculated using image processing software called “Open Drop.” Epoxy droplets were dispensed from 3.240 mm above the substrate. All experiments were conducted at room temperature before curing. The epoxy was then cured at 120°C for 1 hour, inspected, and the curing process continued at 125 °C for an additional 2 hours. The optimal epoxy coverage area was identified after curing using the open-source software “Image-J. In order to analyze the epoxy dispensing further, the epoxy-covered area was measured and compared with the simulation, as shown in Figure 8. The average area covered was compared between simulation and experimental

results, as shown in Table 3. The result indicated that the simulation epoxy-covered area is calculated as 55.36 mm<sup>2</sup>, while the experimental volume is measured at 52.45 mm<sup>2</sup>, resulting in a percentage difference of 5.55%. This comparison results verified that the simulation configuration accurately predicts the epoxy encapsulation process.

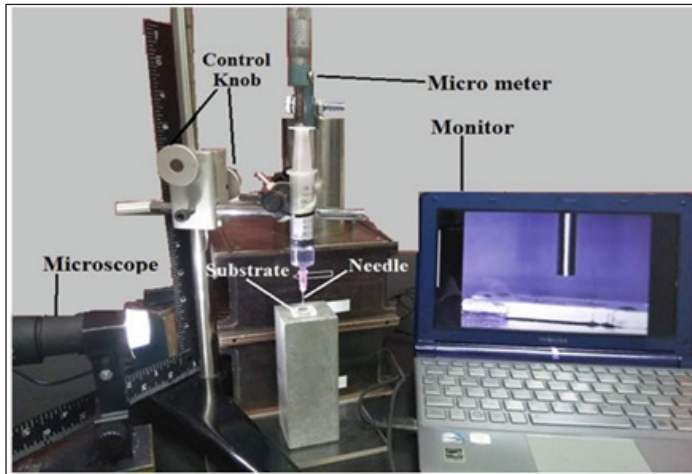


Figure 7. Experimental setup for dispensing the epoxy

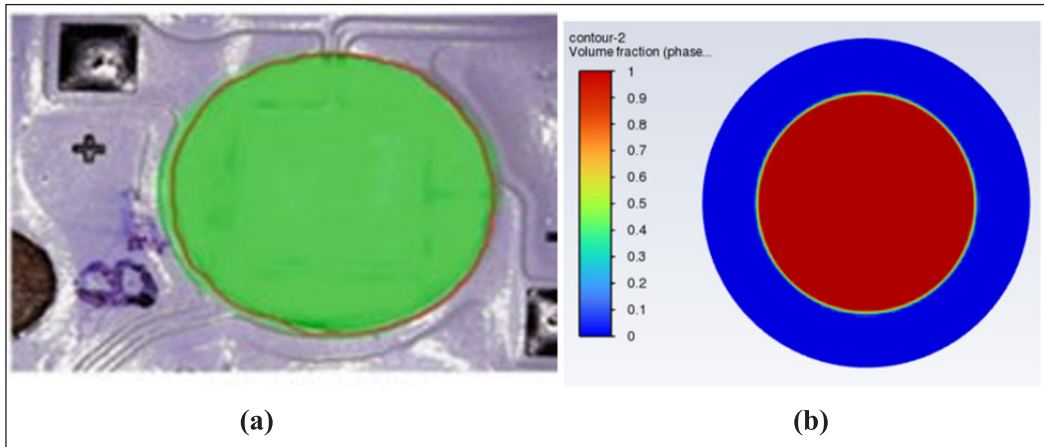


Figure 8. Covered area measurement by (a) Image-J software and (b) Ansys simulation

Table 3  
Comparison of simulation and experimental results

	Experiment	Simulation
Covered Area (mm <sup>2</sup> )	52.45	55.36
Percentage Difference	-	5.55%

## RESULTS AND DISCUSSION

### Effect of Gold Wire Configuration on Maximum Total Deformation

Wire deformation plays a critical role in the reliability of LED assemblies, as misalignment or improper seating of wire bonds can lead to interconnection failures between the LED chip and the substrate. Such failures can disrupt power and signal transmission, compromising LED functionality. Moreover, deformation-induced stresses may degrade the encapsulation material, increasing the risk of cracking or delamination and exposing the LED chip and bonding wires to environmental threats such as moisture and contaminants (Quispe-Aguilar et al., 2023). The maximum total deformation is defined as the largest displacement experienced within the structure to assess the resilience of different wire configurations under load. The stress might cause the encapsulant to crack or delaminate, thereby reducing its ability to protect the LED chip and bonding wires from external elements like moisture and contaminants.

Figure 9 presents a comparison of the maximum total deformation,  $\delta$ , for the gold wire layouts with EMC at a viscosity of 0.448 kg/ms. These differences in deformation can be attributed to the structural characteristics and geometry of each wire design. Type 2 configurations exhibit the largest total deformation at  $9.878 \times 10^{-6}$  mm due to its complex loop structure, which is more susceptible to significant deformations when subjected to external forces or pressure during encapsulation. Following that, the Type 1 configurations rank second in total deformation at  $7.843 \times 10^{-6}$  mm due to their simpler design compared

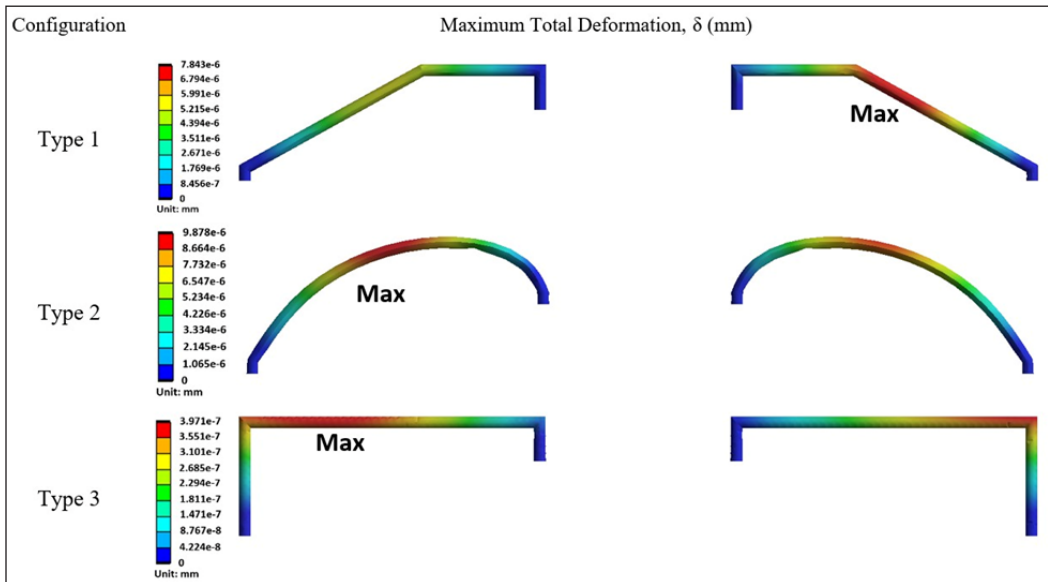


Figure 9. The maximum total deformation of the three types of wire configurations highlights the impact of geometry on deformation behavior

to the Type 2. While it has fewer bends and curves, it still experiences notable deformation due to the inherent flexibility of the wire material. This can be attributed to its specific shape and orientation, which may increase stress concentrations and deformation under applied loads. This can lead to increased stress concentrations in certain regions, consistent with observations in encapsulated interconnects, where encapsulant properties and wire orientation play critical roles in stress distribution (Van Keymeulen et al., 2014).

Lastly, the type 3 wire exhibits the lowest maximum total deformation at  $3.971 \times 10^{-7}$  mm due to the triangular shape influencing its deformation characteristics, balancing structural rigidity and flexibility. The stability and balance of the Type 3 configuration results in a more consistent spread of mechanical stresses throughout the wire. This geometric feature gives the Type 3 configuration an advantage in enduring the forces and pressures encountered during encapsulation, making it more resilient than other configurations. These findings complement prior studies demonstrating that encapsulation geometry can significantly influence deformation behavior, with optimized designs like triangular layouts exhibiting improved durability and mechanical performance (Mosallaei et al., 2018). Furthermore, studies on wire sweep during semiconductor encapsulation highlight the impact of encapsulant viscosity and wire geometry on deformation patterns, reinforcing the importance of shape in mitigating deformation (Han & Wang, 1995). Overall, these findings corroborate existing research on the deformation behaviors of various wire geometries under encapsulation and provide a quantitative comparison of deformation magnitudes. The results emphasize the critical role of wire design in optimizing mechanical performance and minimizing stress concentrations, offering valuable insights for improving encapsulated wire layouts in practical applications.

### **Effect of Gold Wire Configuration on Maximum Equivalent Elastic Strain**

Equivalent elastic strain quantifies the deformation or stretching of the wire material when subjected to external forces during the LED encapsulation process. This strain is essential for evaluating the mechanical strength and reliability of wire connections within an LED device. Figure 10 compares the three wire arrangements based on their largest equivalent elastic strain. The type 2 configuration exhibits the highest equivalent elastic strain at  $4.234 \times 10^{-6}$ . The type 1 configuration demonstrates a maximum equivalent elastic strain of  $3.871 \times 10^{-6}$ . The type 3 configuration has the lowest equivalent elastic strain at  $2.113 \times 10^{-7}$ . As previously noted, the geometric features of the type 3 configuration enhance its structural integrity, providing greater resistance to deformation and strain, which leads to superior elastic behavior compared to other wire configurations. The 90-degree angles in the square shape likely contribute to the wire's increased rigidity, preventing excessive stretching or bending. This structural integrity enables the square-loop wire to retain its shape and resist deformation, resulting in lower elastic strain values, as supported by Wu

and Huang (2011), who found that stronger configurations reduce deformation and strain levels in LED assemblies. They emphasized that structural design significantly impacts mechanical stability, with simpler and well-balanced configurations more resistant to stress and deformation. Additionally, Packwood et al. (2018) examined the effects of varying encapsulant media on wire bond stress under thermal cycling, revealing that stress distribution and deformation levels are highly dependent on material and geometric choices. Their findings underscore the importance of tailoring wire configurations to achieve mechanical stability during encapsulation.

The results confirm trends observed in previous studies and contribute new insights into the impact of specific geometric features, such as the triangular shape in the Type 3 configuration, on strain minimization. This work emphasizes the critical role of wire geometry in ensuring the mechanical reliability of LED assemblies and bridging a gap in understanding how design optimizations translate into practical performance improvements.

#### Effect of Gold Wire Configuration on Maximum von Mises Stress

Von Mises stress represents the equivalent stress at a specific point in a material derived from individual stress components. Monitoring Von Mises stress allows for structural integrity of gold wires to be assessed during encapsulation. High von Mises stress values may reveal areas where the wire is vulnerable to deformation or failure. Thus, understanding von Mises stress in gold wires during LED encapsulation is crucial for gaining insights into the wire's mechanical behavior. Figure 11 compares three-wire configurations in terms of their maximum von Mises stress. The type 2 configuration wire exhibits a maximum von Mises stress of 0.3042 MPa. The type 1 configuration shows a maximum von Mises stress of 0.2811 MPa. Lastly, the type 3 configuration displays a maximum von Mises stress of 0.001547 MPa. Hooke's Law states that stress is directly proportional to strain, a relationship clearly demonstrated in the type 3 configuration, which shows the lowest elastic strain (Figure 10) and the lowest von Mises stress. The higher von Mises stress observed in other wire configurations reflects higher strain levels, thereby increasing the likelihood of mechanical failure. Conversely, lower stress in certain configurations indicates that these wire shapes are more effective at resisting applied forces, helping to maintain structural integrity. The simulation results confirmed that Type 3 wires exhibit the lowest total deformation, equivalent elastic strain, and von Mises stress. This outcome underscores the significant impact of the gold wire's geometrical characteristics on its mechanical properties.

The findings of this study underscore the superior mechanical and stress performance of the Type 2 and Type 3 configurations during the transfer molding process, advancing the understanding of encapsulation mechanics in electronic devices. Notably, the observation that the Type 2 configuration exhibited the highest equivalent elastic strain and von Mises stress aligns with findings by Tian et al. (2019), who reported reduced signal transmission

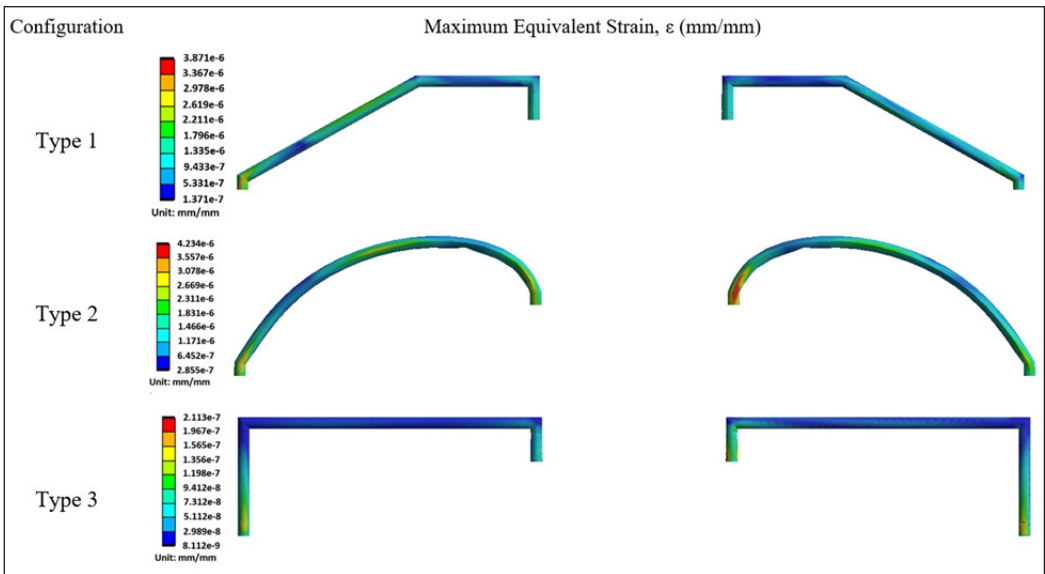


Figure 10. The maximum equivalent strain of the three types of wire configurations highlights the impact of geometry on strain behavior

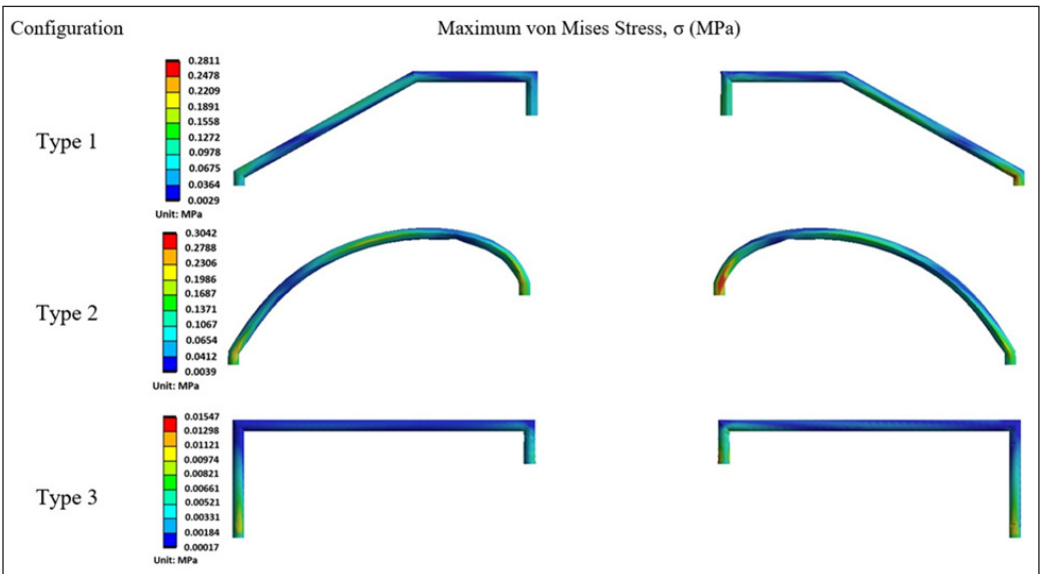


Figure 11. The maximum von Mises stress of the three types of wire configurations highlights the impact of geometry on stress behavior

quality (34.32%) in the Type 2 configuration compared to the Type 1 configuration (36.69%) under similar conditions. This suggests that while Type 2 configurations endure higher stress levels, they may trade off performance in electrical signal integrity.

Furthermore, the results indicate that the Type 3 configuration demonstrates superior resilience with the lowest maximum total deformation, equivalent elastic strain, and von Mises stress. This aligns with the findings of Choube and Sambhe (2020), who found that square cross-section springs outperformed rectangular cross-sections in stress scenarios. This correlation directly supports the effectiveness of the square-loop Type 3 configuration in mitigating mechanical and thermal stresses encountered during LED encapsulation processes. These comparisons illustrate how the present study builds on prior research by reinforcing the significance of wire geometry in stress distribution and encapsulation efficiency. Specifically, it confirms the advantages of the Type 3 configuration in mechanical performance and its potential for improved reliability under operational stresses.

## CONCLUSION

This study focussed on investigating the impact of wire bonding looping formation on the LED encapsulation process. This numerical study used a fluid with a viscosity of 0.448 kg/ms aligned with experiments using EMC with the same viscosity. Both simulation and experimental data indicated that The comparison results verified that the simulation configuration accurately predicted the epoxy encapsulation process with a 5.55% volume difference, confirming the accuracy of the simulation configuration.

Three gold wire designs were evaluated with EMC at 0.448 kg/ms viscosity for deformation, equivalent elastic strain and maximum von Mises stress. The type 2 wire demonstrated good compatibility with EMC during LED encapsulation, exhibiting the highest deformation, equivalent elastic strain and von Mises stress among the three designs. The Type 1 wire showed better performance than the Type 2 wires in terms of maximum total deformation, equivalent elastic strain, and von Mises stress. However, the Type 3 wire emerged as the optimal gold wire topology for LED encapsulation due to its low maximum total deformation, equivalent elastic strain, and von Mises stress, highlighting its efficacy in LED encapsulation processes.

## ACKNOWLEDGEMENTS

This work was supported by the Ministry of Higher Education (MoHE) Malaysia for the Fundamental Research Grant Scheme with Project Code: FRGS/1/2022/TK10/USM/03/11

## REFERENCES

- Alim, M. A., Abdullah, M. Z., Aziz, M. S. A., & Kamarudin, R. (2021). Die attachment, wire bonding, and encapsulation process in LED packaging: A review. *Sensors and Actuators A: Physical*, 329, Article 112817. <https://doi.org/10.1016/j.sna.2021.112817>
- Alim, M. A., Abdullah, M. Z., Aziz, M. S. A., Kamarudin, R., Irawan, A. P., & Siahaan, E. (2020). Experimental study on luminous intensity of white LEDs of different configurations. *IOP Conference Series: Materials Science and Engineering*, 1007(1), Article 012145. <https://doi.org/10.1088/1757-899X/1007/1/012145>

- Arriola, E. R., Ubando, A. T., Gonzaga, J. A., & Lee, C. C. (2023). Wafer-level chip-scale package lead-free solder fatigue: A critical review. *Engineering Failure Analysis*, *144*, Article 106986. <https://doi.org/10.1016/j.engfailanal.2022.106986>
- Azmi, M. A., Abdullah, M. K., Abdullah, M. Z., Ariff, Z. M., Ismail, M. A., & Aziz, M. S. A. (2018). Flow behavior analysis of EMC in molded underfill (MUF) encapsulation for multi flip-chip package. *Journal of Physics: Conference Series*, *1082*(1), Article 012015. <https://doi.org/10.1088/1742-6596/1082/1/012015>
- Azrain, M. M., Omar, G., Mansor, M. R., Fadzullah, S. H. S. M., & Lim, L. M. (2019). Failure mechanism of organic light emitting diodes (OLEDs) induced by hygrothermal effect. *Optical Materials*, *91*, 85–92. <https://doi.org/10.1016/j.optmat.2019.03.003>
- Baek, J. H., Park, D. W., Oh, G. H., Kawk, D. O., Park, S. S., & Kim, H. S. (2022). Effect of cure shrinkage of epoxy molding compound on warpage behavior of semiconductor package. *Materials Science in Semiconductor Processing*, *148*, Article 106758. <https://doi.org/10.1016/j.mssp.2022.106758>
- Choube, A. M., & Sambhe, R. U. (2020). Stress analysis of square and rectangular cross section helical spring. *International Journal of Scientific Research in Science, Engineering and Technology*, *7*(1), 1–6.
- Garoosi, F., & Mahdi, T. F. (2022). Numerical simulation of three-fluid Rayleigh-Taylor instability using an enhanced Volume-Of-Fluid (VOF) model: New benchmark solutions. *Computers & Fluids*, *245*, Article 105591. <https://doi.org/10.1016/j.compfluid.2022.105591>
- Hamidnia, M., Luo, Y., & Wang, X. D. (2018). Application of micro/nano technology for thermal management of high power LED packaging – A review. *Applied Thermal Engineering*, *145*, 637–651. <https://doi.org/10.1016/j.applthermaleng.2018.09.078>
- Han, S., & Wang, K. K. (1995). A study on wire sweep in encapsulation of semiconductor chips using simulated experiments. *Journal of Electronic Packaging*, *117*, 178–184. <https://doi.org/10.1115/1.2792089>
- Koutchma, T. (2019). Technology of LED light sources and systems from visible to UV range. In *Ultraviolet LED Technology for Food Applications* (pp. 25–33). Elsevier. <https://doi.org/10.1016/B978-0-12-817794-5.00002-9>
- Lee, M., Park, G., Park, C., & Kim, C. (2020). Improvement of grid independence test for computational fluid dynamics model of building based on grid resolution. *Advances in Civil Engineering*, *2020*(1), Article 8827936. <https://doi.org/10.1155/2020/8827936>
- Mahmood, S., Kant, C., Raj, A., Lin, H. C., & Katiyar, M. (2022). Evaluation of encapsulation strategies for solution-processed flexible organic light-emitting diodes. *Materials Chemistry and Physics*, *292*, Article 126808. <https://doi.org/10.1016/j.matchemphys.2022.126808>
- Montoya, F. G., Peña-García, A., Juaidi, A., & Manzano-Agugliaro, F. (2017). Indoor lighting techniques: An overview of evolution and new trends for energy saving. *Energy and Buildings*, *140*, 50–60. <https://doi.org/10.1016/j.enbuild.2017.01.028>
- Moon, S. H., Park, Y. W., & Yang, H. M. (2017). A single unit cooling fins aluminum flat heat pipe for 100 W socket type COB LED lamp. *Applied Thermal Engineering*, *126*, 1164–1169. <https://doi.org/10.1016/j.applthermaleng.2016.11.077>

- Mosallaci, M., Jokinen, J., Kanerva, M., & Mäntysalo, M. (2018). The effect of encapsulation geometry on the performance of stretchable interconnects. *Micromachines*, 9(12), Article 645. <https://doi.org/10.3390/mi9120645>
- Packwood, M., Li, D., Mumby-Croft, P., & Dai, X. (2018). Thermal simulation into the effect of varying encapsulant media on wire bond stress under temperature cycling. In *2018 19th International Conference on Electronic Packaging Technology (ICEPT)* (pp. 152–155). IEEE Publishing. <https://doi.org/10.1109/ICEPT.2018.8480816>
- Quispe-Aguilar, M., Aparco, R., Otero, C., Huamán, M., & Huamán-Romani, Y. (2023). A probabilistic Bayesian machine learning framework for comprehensive characterization of bond wires in IGBT modules under thermomechanical loadings. *Journal of Electronic Materials*, 53(1), 123–134. <https://doi.org/10.1007/s11664-023-10868-y>
- Roslan, H., Aziz, M. S. A., Abdullah, M. Z., Kamarudin, R., Ishak, M. H. H., Ismail, F., & Irawan, A. P. (2020). Analysis of LED wire bonding during encapsulation process. *IOP Conference Series: Materials Science and Engineering*, 1007(1), Article 012173. <https://doi.org/10.1088/1757-899X/1007/1/012173>
- Shan, X., & Chen, Y. (2018). Experimental and modeling study on viscosity of encapsulant for electronic packaging. *Microelectronics Reliability*, 80, 42–46. <https://doi.org/10.1016/j.microrel.2017.11.011>
- Tian, W., Cui, H., & Yu, W. (2019). Analysis and experimental test of electrical characteristics on bonding wire. *Electronics*, 8(3), Article 365. <https://doi.org/10.3390/electronics8030365>
- Ünal, D., Varol, S. F., Brault, J., Chenot, S., Al Khalfioui, M., & Merdan, Z. (2022). Improved performance of near UV-blue n-ZnO/p-GaN heterostructure LED with an AlN electron blocking layer. *Microelectronic Engineering*, 262, Article 111830. <https://doi.org/10.1016/j.mee.2022.111830>
- Van Keymeulen, B., Gonzalez, M., Bossuyt, F., De Baets, J., & Vanfleteren, J. (2014). Mechanical analysis of encapsulated metal interconnects under transversal load. In *2014 15th International Conference on Thermal, Mechanical and Mult-Physics Simulation and Experiments in Microelectronics and Microsystems (EuroSimE)* (pp. 1-8). IEEE Publishing. <https://doi.org/10.1109/EurosimE.2014.6813842>
- Wu, F. T., & Huang, Q. L. (2011). A precise model of LED lighting and its application in uniform illumination system. *Optoelectronics Letters*, 7(5), 334-336. <https://doi.org/10.1007/s11801-011-1031-x>